JGR Atmospheres

RESEARCH ARTICLE
10.1029/2023JD039228

The Role of Topography in Controlling Evapotranspiration Age

Chen Yang[1,2], Reed Maxwell[1,2,3], Jeffrey McDonnell[4,5], Xiaofan Yang[6], and Danielle Tijerina-Kreuzer[1,2]

[1]Department of Civil and Environmental Engineering, Princeton University, Princeton, NJ, USA, [2]Integrated GroundWater Modeling Center, Princeton University, Princeton, NJ, USA, [3]High Meadows Environmental Institute, Princeton University, Princeton, NJ, USA, [4]School of Environment and Sustainability, Global Institute for Water Security, University of Saskatchewan, Saskatoon, SK, Canada, [5]School of Geography, Earth and Environmental Sciences, University of Birmingham, Birmingham, UK, [6]Faculty of Geographical Science, State Key Laboratory of Earth Surface Processes and Resource Ecology, Beijing Normal University, Beijing, China

Key Points:

- Particle tracking based on integrated hydrologic modeling suggests the role of groundwater in Evapotranspiration (ET) age variations at the regional scale
- Topography-driven Tóthian subsurface flow shapes the basic spatiotemporal patterns of ET age
- Where water table depths are between 1 and 10 m, ET age has a high temporal variability due to the seasonal use of groundwater by ET

Supporting Information:

Supporting Information may be found in the online version of this article.

Correspondence to:

C. Yang,
cy15@princeton.edu

Citation:

Yang, C., Maxwell, R., McDonnell, J., Yang, X., & Tijerina-Kreuzer, D. (2023). The role of topography in controlling evapotranspiration age. *Journal of Geophysical Research: Atmospheres*, *128*, e2023JD039228. https://doi.org/10.1029/2023JD039228

Received 10 MAY 2023
Accepted 1 SEP 2023

Abstract Evapotranspiration (ET) age is a key metric of water sustainability but a major unknown partly due to the extreme difficulty in modeling it. Groundwater is found to be important in ET age variations in small-scale studies, yet our understanding is insufficient because groundwater systems are nested across scales. Here, we conducted GPU-accelerated particle tracking with integrated hydrologic modeling to quantify the variations in ET age at a regional scale of ~0.4 M km^2. Simulation results reveal topography-driven flow paths shaping the spatial and temporal patterns of ET age variations. On ridges, where root zone decoupling with deep subsurface storage, ET age is generally young, with seasonal variations dominated by meteorological conditions. In the valley bottom, ET age is generally old, with significant subseasonal variations caused by the convergence of subsurface flow paths. On hillslopes with water table depths ranging from 1 to 10 m, ET age shows strong seasonal variations caused by the connections with lateral groundwater regulated by ET demand. Our modeling approach provides insights into the basic linkages between ET age and topography at large scale. Our work highlights the perspective of multiscale studies of ET age, suggesting new field experiments to test these process connections and to determine if such linkages warrant inclusion in Earth System Models.

Plain Language Summary Evapotranspiration (ET) is a major component of the hydrological cycle, and ET age is the time that water takes from precipitation to move through the subsurface and, ultimately, to soil evaporation and/or plant water uptake. A modeling approach for ET age at regional scales is lacking in the hydrologic community, which partly hinders the scientific progress of ET age. Here, we develop a new modeling approach for ET age using particle tracking with an integrated hydrologic model. We conducted a 42-year particle tracking simulation in the Haihe River Basin. Our simulation results showed significant topographic controls on ET age variations due to the topography-driven subsurface flow paths. Simulation results also showed that ET water increased in age from the ridges to valleys throughout our model domain due to the increasing contributions from groundwater. In areas where water table depths vary between 1 and 10 m, the simulated ET age shows the strongest seasonal variability. We hope that our findings can guide the design of new field experiments to test these topographic controls on ET age so that, ultimately, we can include such functions in Earth System Models of land surface processes.

1. Introduction

Evapotranspiration (ET) is the largest terrestrial water flux (Schlesinger & Jasechko, 2014) and is vital for understanding and modeling the terrestrial water cycle (Maxwell & Condon, 2016). But while ET flux tells us the gross quantity of ET water (i.e., *how much* water), it does not tell us about its source, pathway, and age (i.e., *which* water) (Benettin et al., 2021; Kuppel et al., 2020). Indeed, ET age is now seen as a crucial descriptor of the time water takes from precipitation to its movement through the subsurface and ultimately to plant water uptake and soil evaporation (Botter, 2012; Kuppel et al., 2020). Once thought to be simple, the fundamental mechanisms governing variations in ET age remain unclear (Benettin et al., 2021; Botter, 2012) with cryptic connections and disconnections of ET with the subsurface waters, for example, the groundwater (Fan, 2016; McDonnell, 2017).

Recent studies have used tracer experiments (Benettin et al., 2021; Nehemy et al., 2021; Sprenger et al., 2019), analytical approaches (Botter, 2012; Calabrese & Porporato, 2017), and column/hillslope numerical models (Asadollahi et al., 2022; Maxwell et al., 2019; Rahimpour Asenjan & Danesh-Yazdi, 2020; Sprenger et al., 2018)

to address many aspects of ET age. However, the limited spatiotemporal sampling, lumped conceptualization, and truncated modeling domain of these approaches limit our ability to connect this work to model estimates of groundwater age distributions (Engdahl & Maxwell, 2014) and streamflow travel time distributions (TTDs) (Kirchner, 2016a, 2016b; Maxwell et al., 2016). Clearly, our understanding of ET age lags far behind our understanding of groundwater and streamflow ages (Botter, 2012; Soulsby et al., 2016). Lateral heterogeneities in space and their temporal dynamics should be considered to improve understanding of the ET age variations (Kuppel et al., 2020).

The emergence of distributed numerical models tracking water movement at the catchment scale has facilitated the mechanistic assessment of ET age variations by integrating lateral heterogeneities and interactions (Knighton et al., 2020; Kuppel et al., 2018, 2020; Wilusz et al., 2019). With the distributed modeling approach, Kuppel et al. (2020) and Wilusz et al. (2019) showed a higher baseline of ET age at the valley bottom of the catchment. Such unintentional results may imply some intrinsic ET age variations differentiated by the locations in the catchment yet lack enough attention and further exploration. Given that groundwater plays an important role in ET age variations at the stand scale, the spatially nested Tóthian groundwater flow (Tóth, 1963) controlled by topography may regulate ET age variations across multiple scales. The numerical domains in these previous studies using distributed models are thus far mainly headwater catchments. Given that the Tóthian groundwater flow systems are multi-level across scales, that is, local, intermediate, and regional systems, these previous small-scale studies may not be enough. A full view of spatiotemporal variations in ET age at larger scales may be necessary to better understand the role of lateral groundwater in governing these variations.

As a result, we leverage the latest parallel architecture of the multi-GPU (Yang et al., 2021; Yang et al., 2023a, 2023b; Yang, Maxwell, McDonnell, et al., 2022; Yang, Maxwell, & Valent, 2022) to develop a GPU-accelerated particle tracking approach linked to the integrated hydrologic modeling. We explicitly simulate flow paths and ET age at the regional scale with an explicit treatment of three-dimensional groundwater flow and ET at an hourly time step. Previous modeled soil-water mass balances at large scales have pointed to drainage position (i.e., location on the topographic gradient) as a control on plant water uptake where upland plants may rely on deep soil-water and lowland plants use convergent, lateral groundwater (Fan et al., 2017; Miguez-Macho & Fan, 2021). Here, we conduct a 42-year particle tracking simulation for the ~0.4 M km^2 Haihe River Basin to explore the effects of topography-driven groundwater flow paths on the spatial and temporal variations in ET age. Our specific questions guiding the application of our new tool are:

1. Does ET age show systematic variations with topography?
2. Where and when are such topographic controls the most significant?

Our work brings new tools (i.e., our GPU-accelerated particle tracking approach linked to integrated hydrologic modeling) to test the topography-ET age connection in a regional watershed. We also leverage the known Tóthian concepts (Tóth, 1963), known topographic controls on groundwater age distributions (Gomez & Wilson, 2013; Jiang et al., 2010) and TTDs of streamflow (Cardenas, 2008; Rodriguez et al., 2020), and past numerical modeling (Cardenas, 2008; Gomez & Wilson, 2013; Jiang et al., 2010) and tracer data analysis (Rodriguez et al., 2020) that links to our conceptual thinking regarding the topographic controls on groundwater age and streamflow TTDs. We use this combination of the latest modeling tools and reflection on past concepts and tracer findings to unravel how the topography-driven flow paths affect ET age at the large watershed scale.

2. Methods

2.1. Study Area

The modeling domain (112.70°–117.28°E and 34.44°–41.01°N) located in Northern China (Figure S1 in Supporting Information S1) covers most of the Haihe River Basin and a small portion of the Yellow River Basin. It encompasses the Taihang and Yanshan mountain ranges and most of the North China Plain (Figure S2a in Supporting Information S1). Elevations range from 0 to 2,800 m (Rabus et al., 2003) (Figure S2b in Supporting Information S1). Annual precipitation, annual evaporation, and annual mean temperature are 539 mm, 470 mm, and 9.6°C (1951–2007), respectively (Bao et al., 2012; Chu et al., 2010; Zheng et al., 2009). Land cover types are mainly croplands in plains, while the mountainous headwater areas are dominated by a mix of forests, croplands, shrublands, and grasslands (USGS, 2018) (Figure S2c in Supporting Information S1). Soil types are mainly silt loam in plains and loam-dominant in mountainous areas (Shangguan et al., 2012) (Figure S2d in Supporting

Information S1). The plains and valleys are dominated by Quaternary sediments together with outcrops of crystalline and carbonate rocks in ridge areas (Gleeson et al., 2011) (Figure S2e in Supporting Information S1).

2.2. Numerical Models and Simulations

We use the integrated hydrologic model ParFlow-CLM (PF-CLM) (Kuffour et al., 2020; Maxwell & Miller, 2005). ParFlow (PF) integrates the two-dimensional overland flow using the kinematic wave approximation and the three-dimensional variably saturated subsurface flow by Richards' equation and then couples an advanced Common Land Model (CLM) via the root zone for vegetation and land-energy processes (Maxwell & Condon, 2016). The PF-CLM model for this study area is modified from our previous work (Yang et al., 2020), where the meteorological forcing is changed from 1.25° gridded Japanese 55-year reanalysis (JRA-55) (Harada et al., 2016; Kobayashi et al., 2015) to 0.25° gridded ECMWF reanalysis v5 (ERA5) (Hersbach et al., 2018) (Figure S3 in Supporting Information S1). The spatial resolution is changed from approximately 1 km to rigorous 1 km. The model comprises five vertical layers of 100, 1, 0.6, 0.3, and 0.1 m thicknesses from bottom to top, where the upper 2 m is coupled with CLM. Thus, the modeling domain has a dimension of 509 km × 921 km × 102 m with 2,343,945 (509 columns × 921 rows × 5 layers) grid cells. After a full spin-up of the PF model, ensuring that the storage change in the modeling domain is less than 3% of the precipitation minus ET (Maxwell et al., 2015), the PF–CLM model was spun up for another 3 years at an hourly time step using the meteorological forcing of 1979, a time period before disturbance (e.g., groundwater pumping) by human activities on our modeling domain.

EcoSLIM is a Lagrangian particle tracking code that works seamlessly with PF-CLM to simulate the advection and diffusion of water parcels in the subsurface (Maxwell et al., 2019). It was developed to calculate water ages (groundwater, ET, and outflow) and diagnose source water composition (snow, rainfall, and historical groundwater). It was recently accelerated by multi-GPU (Yang et al., 2021; Yang et al., 2023a, 2023b; Yang, Maxwell, & Valent, 2022), thus enabling particle tracking at the regional scale, which is computationally expensive and previously infeasible. Results of the third-year spin-up from the PF-CLM model were repeatedly used to spin-up the EcoSLIM model for a further 42 years at an hourly time step. We used the results of Wang et al. (2018), who sampled groundwater from wells at depths between 2 and 90 m in the mountainous area in our modeling domain and got apparent groundwater ages of these samples from 24 to 42.5 years based on CFC-12 and 25.5–42 years based on CFC-113. Using this field information to guide our model analysis, we stopped the EcoSLIM spin-up at the end of the 42nd year.

The boundary conditions applied were no-flux, except the uppermost model layer, which is open for the entrance and exit of particles as precipitation and ET. In each grid cell, one particle was inserted in the initialization, representing the historical groundwater. At each time step, particles were removed when and where the PME (precipitation minus ET) was negative or exited as outflow once they reached the stream. One particle was added into a grid cell based on the accumulated positive PME each day. Notwithstanding, the total number of particles in the 42nd year was around 250 million, beyond any previous particle tracking studies that we are aware of. Our model work was evaluated by comparing snow water equivalent (SWE), sensible and latent heat fluxes, and streamflow with reanalysis data, and comparing water table depth (WTD) with data from previously published studies (Figures S4–S6 in Supporting Information S1). Simulated ET and streamflow ages were compared with the general understanding collected from previous studies (Figure S7 in Supporting Information S1). Note that evaluation of the large-scale hydrologic model is challenging (Gleeson et al., 2021), and the evaluation of water ages at such a large scale is almost impossible. Our evaluation confirms the capability of our model to suggest general patterns of water age variations in the modeled domain. Our model may be treated as a virtual model approximating the real world with our current best efforts. Our results are suggestions from our simulation results and may not be the world's truth, given that the ET age is still an emerging field without a complete theoretical basis. Please refer to Texts S1–S3 in Supporting Information S1 for details of the model setup and uncertainties and limitations of the simulation results.

2.3. Analysis

We calculated annually aggregated ET age in space using particles that exited as ET in the 42nd year of simulation. For each grid cell in the root zone, if the number of particles that exited as ET in the year was greater than zero, then its annually aggregated ET age was determined by

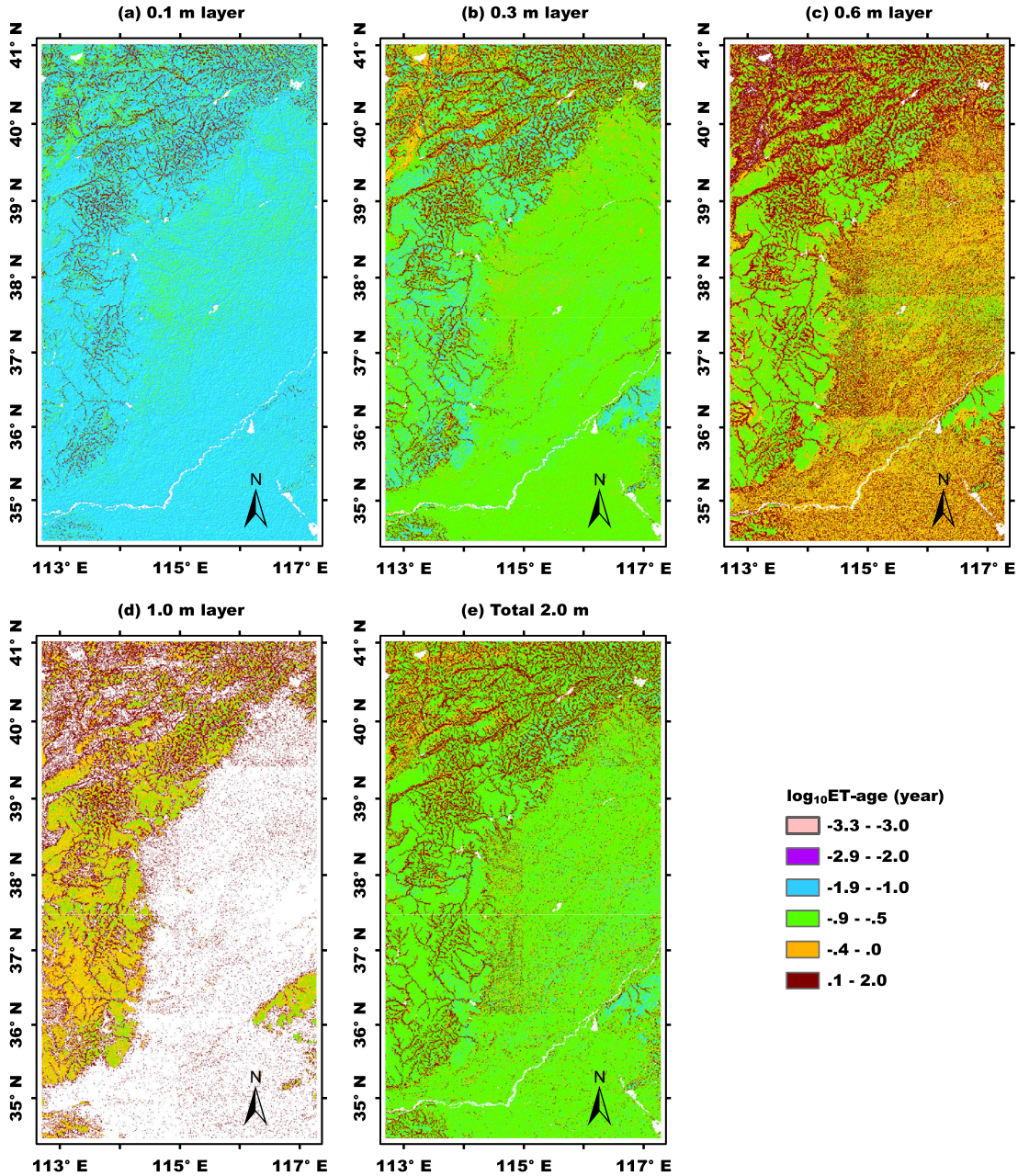

Figure 1. Annually aggregated distributions of evapotranspiration (ET) age for each of the upper four layers (a–d) and the whole root zone (e). The values missing in plains and northwestern mountainous areas in the 1.0 m layer (d) are due to the limited root fractions of croplands at such a depth (Dai et al., 2003).

$$Age(i,j,k) = \frac{\sum_{n=1}^{N(i,j,k)} Age_n m_n}{\sum_{n=1}^{N(i,j,k)} m_n}, 1 \le n \le N(i,j,k) \quad (1)$$

where $Age(i, j, k)$ is the annually aggregated ET age in grid cell (i, j, k), $N(i, j, k)$ is the total number of particles exited as ET from grid cell (i, j, k) in the whole year, and m_n and Age_n are the mass and the age of particle n, respectively. The results based on Equation 1 are used for plotting Figure 1.

Particles that exited as ET at time t in the entire modeling domain were used to calculate spatially aggregated ET age $Age(t)$ using

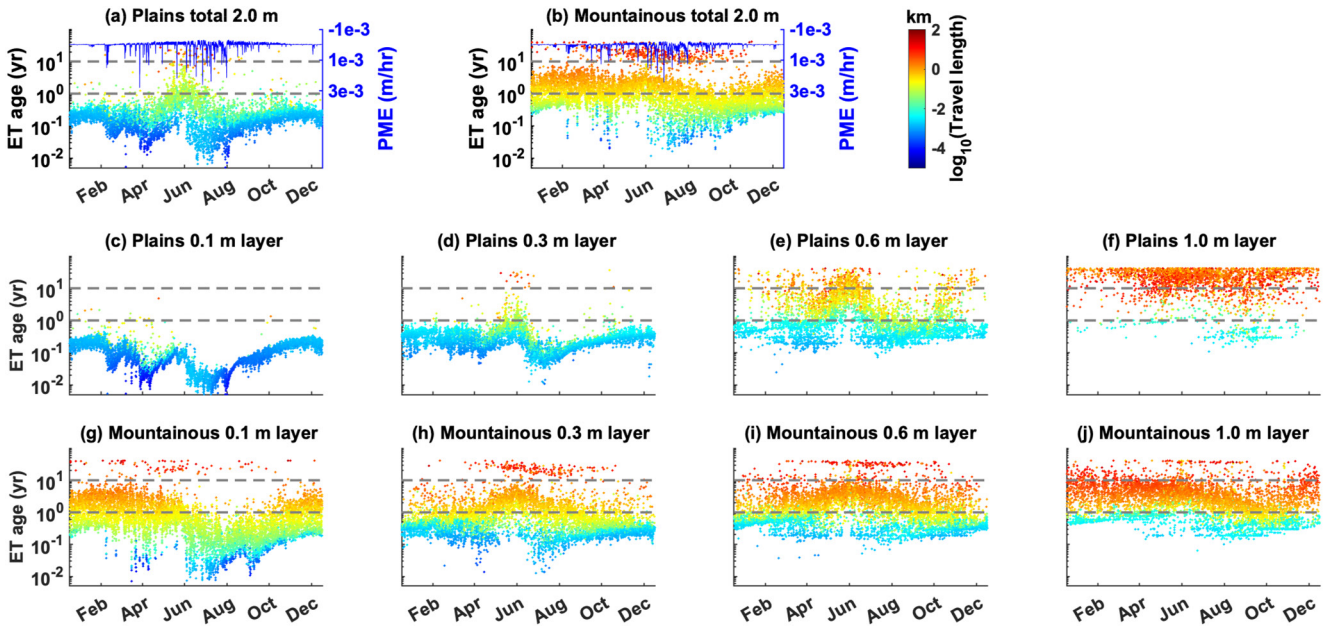

Figure 2. Temporal variations of spatially aggregated evapotranspiration (ET) age in the 42nd year for the plains (a) and the mountainous area (b). Plains and mountainous areas are differentiated based on Figure S2a in Supporting Information S1. The first row is for the whole root zone, while the second and third are for different model layers in each region: the second row is for the plains, while the third row is for the mountainous area. In the second and third rows (from left to right), the panels are the 0.1 m, 0.3 m, 0.6 m, and 1.0 m layers in the root zone, respectively. ET ages are mass-weighted ages and are colored by mass-weighted travel lengths. The ET age and travel length in this figure are calculated based on Equation 2 in the main text. Precipitation minus ET (PME) in each region is indicated in (a) and (b) by blue lines representing spatially averaged variations. Two dash lines in each plot indicate ages of 1 year and 10 years, respectively.

$$Age(t) = \frac{\sum_{n=1}^{N(t)} Age_n m_n}{\sum_{n=1}^{N(t)} m_n}, 1 \le n \le N(t) \quad (2)$$

ET ages in the mountainous areas and plains are differentiated by separating ET particles at time t into two portions based on their spatial coordinates (Figure S2a in Supporting Information S1) and then applying Equation 2 to each portion. Similarly, ET ages in mountainous areas were further distinguished by critical WTD as proposed by Kollet and Maxwell (2008) for three mountainous subregions. The results based on Equation 2 are used for plotting Figures 2 and 3. Subsurface travel lengths of ET water were calculated using the same method as ET age. Ages and lengths of subsurface storage are reported in Supporting Information S1.

3. Results

3.1. Spatial and Temporal Variations in ET Age

Our simulation results show, perhaps not surprisingly, that ET age is younger in recharge areas and older around streams (Figure 1 and Figure S6a in Supporting Information S1 shows locations of streams). Such variations persist across the modeling domain, suggesting distinct topography-driven patterns in ET age, despite high variabilities in land cover types, soil types, geologic units, and meteorological conditions (Figures S2 and S3 in Supporting Information S1). In addition, ET age increases with depth except for groundwater convergence regions where ET is old (>1 year) across the whole root zone due to groundwater upwelling. Temporally, a significant vertical gradient in ET age with depth exists in plains (the baseline excluding the peak in Figures 2c–2f): ET age increases from $<10^{-1}$ year (hours to days) in 0.1 m layer to > 10 years in 1 m layer. In contrast, large fluctuations at small time scales (subseasonal) characterize ET age variations in the mountainous areas of our domain: ET age frequently switches between old and young (Figures 2g–2j). Please see Section 4 for a discussion of controls on these variations from flow paths. Moreover, our simulated year showed a large increase in ET age of up to ~42 years in plains between April and June (Figure 2a). Forty-two year is the maximum age permitted in this study due to the total simulation time, so this age could likely be much larger.

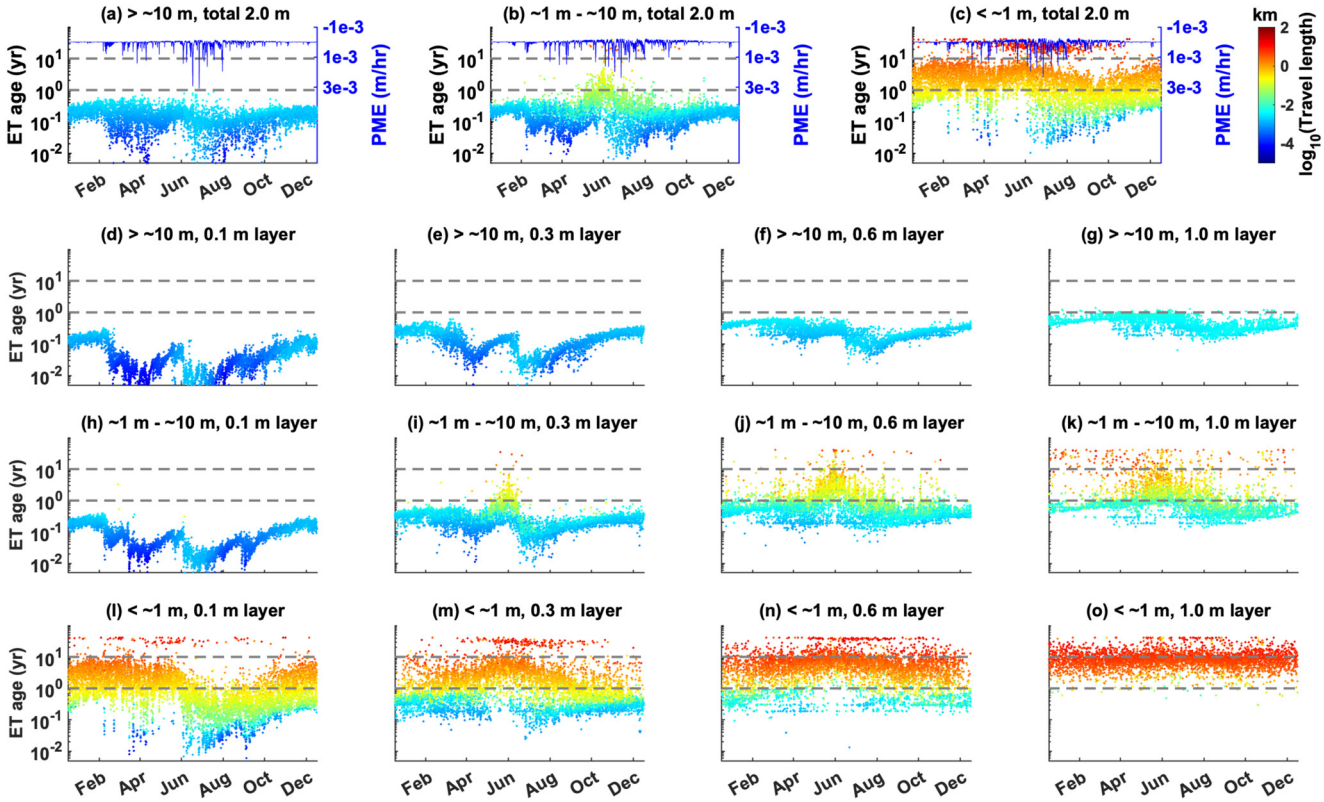

Figure 3. Temporal variations of spatially aggregated evapotranspiration (ET) age in the 42nd year in different subregions of the mountainous areas. The division of subregions here is based on water table depth (WTD): the subregion with WTD < 1 m (a), the subregion with WTD between 1 and 10 m (b), and the subregion with WTD > 10 m (c). The first row is for the whole root zone, while the second to fourth are for different model layers in each subregion. In the second to fourth rows (from left to right), the panels are the 0.1 m, 0.3 m, 0.6 m, and 1.0 m layers in the root zone, respectively. ET ages are mass-weighted ages and are colored by mass-weighted travel lengths. The ET age and travel length in this figure are calculated based on Equation 2 in the main text. Precipitation minus ET (PME) in each subregion is indicated in (a–c) by blue lines representing spatially averaged variations. Two dash lines in each plot indicate ages of 1 year and 10 years, respectively.

Kollet and Maxwell (2008) pointed out that, in the zone with WTD between 1 and 10 m, water and energy fluxes show the most interactions between land surface processes and groundwater. Therefore, we further divided the mountainous areas into three subregions based on WTD (WTD > 10 m, 1 m < WTD < 10 m, and WTD < 1 m) to check if the simulated ET ages also obey this critical depth theory. On ridges (WTD > 10 m) (Figures 3a and 3d–3g), the 2 m root zone, much smaller than the WTD of 10 m, is not connected to groundwater. Precipitation inputs are generally drained vertically in the unsaturated zone. Consequently, ET age is young throughout the entire root zone, varying from $<10^{-1}$ year (hours to days) at the top root zone (i.e., the 0.1 m layer in Figure 3d) to $<10^{0}$ year (several months) at the bottom root zone (i.e., the 1 m layer in Figure 3g). Seasonal variations in ET age with meteorologic shifts between wet and dry (i.e., variations of PME in Figure 3a) are obvious near the land surface, while such variations are largely damped in the deep root zone (Figures 3d–3g). On hillslopes (1 m < WTD < 10 m) (Figures 3b and 3h–3k), ET age shows strong seasonal variability through the complete root zone (Figures 3h–3k), which is similar to that in plains (Figures 2c–2f) where a large portion of WTDs are also located between ~1 and 10 m (Figure S6 in Supporting Information S1). In valley bottoms (WTD < 1 m) (Figures 3c and 3l–3o), ET ages are characterized by old water ($>10^{0}$ year) with significant fluctuations at subseasonal timescales. Note that ET age variations in this subregion (Figures 3c and 3l–3o) show the highest similarity to that of the whole mountainous area (Figures 2b and 2g–2j), implying that ET age variations in groundwater convergence zones dominate throughout the mountainous areas.

3.2. Key Zone of ET Age Variations

We build a relationship between the subsurface travel length and the depth of the water source in the modeling area based on simulation results; in other words, the longer the travel length, the deeper the water source (Text S4 and Figure S8 in Supporting Information S1). We define the water with subsurface travel lengths longer than

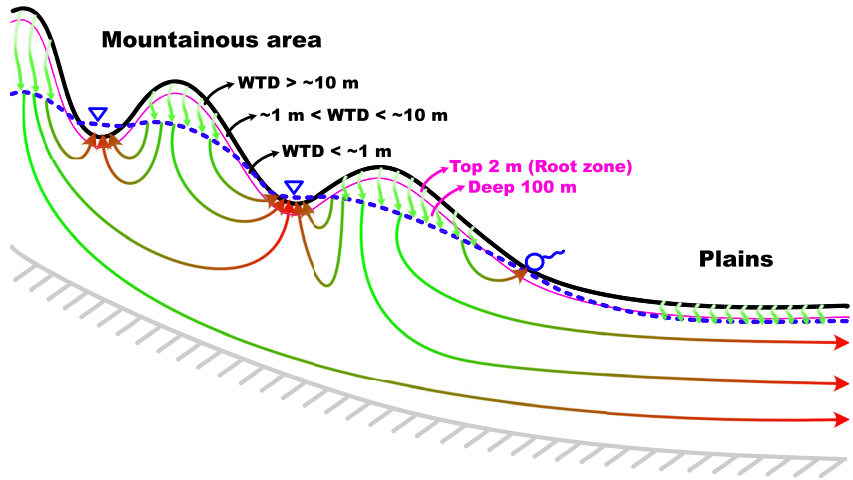

Figure 4. Conceptual diagram of topography-driven flow paths in the modeling domain based on the Tóthian concept. Mountainous areas and plains are dominated by rolling and flat topographies, respectively. The top 2 m represents the upper four layers of the model, that is, the root zone. The deeper 100 m is the bottom layer of the model. Three subregions in the mountainous areas differentiated by water table depth (WTD) are exemplified. These subregions represent the ridges with WTD larger than ~10 m, the hillslopes with WTD between ~1 m and ~10 m, and the valleys with WTD smaller than ~1 m.

10 km as "lateral groundwater", indicating groundwater from the deep subsurface storage (see further details in Text S4 and Figure S9 in Supporting Information S1). In plains and on hillslopes (Figures 2c–2f and 3h–3k), where ET age shows highly seasonal variability, the increase in travel length (colored in Figures 2 and 3) of the ET water highlights the critical importance of groundwater to meet seasonal ET demand.

During the April to June period, precipitation minus ET (PME) is negative (Figure 2a), indicating limited precipitation with strong ET. The maximum absolute value of negative PME in Figure 2a is 3.20×10^{-4} m/hr (2,803 mm/year or 7.68 mm/day), representing the strongest ET flux, while the annual average magnitude of negative PME is 2.94×10^{-5} m/hr (258 mm/year or 0.71 mm/day). These values are comparable to the annual average groundwater pumping rate of 6.85×10^{-5}–9.13×10^{-5} m/hr (600–800 mm/year) in the piedmont area in the North China Plain, a worldwide hotspot of groundwater depletion (Cao et al., 2013). Hence, ET age in this subregion (1 m < WTD < 10 m) is controlled by shallow precipitation inputs and deep groundwater subsidy. The nonlinear shift of ET age to 42 years (e.g., Figure 3k) instead of a more progressive increase with time implies a switching of ET source water to sources deeper than the 2 m root zone during periods of water stress. In other words, plants in their rooting area use groundwater that upwells into the root zone like a seasonal extraction.

In the valley bottom, the extraction of groundwater by plants is insignificant due to the abundant water in such stable discharge areas. Slight increases in ET age were observed in the second and third WTD layers during dry conditions due to precipitation recharge deficits (Figures 3m and 3n). In contrast, on ridges (Figures 3d–3g), the short travel lengths indicate the decoupling of the root zone with the deep subsurface storage. Seasonal variations of ET age are largely mediated by meteorologic variations.

4. Discussion and Conclusions

Figure 4 presents a conceptual model for the topography-driven flow paths and ET ages in the modeling domain, influenced by previous work (Fan, 2015; Freeze & Witherspoon, 1967; Maxwell et al., 2016; Tóth, 1963; Zhang et al., 2021). It contrasts how rolling and flat topography in complex topography differentiates water flow paths. In mountain valleys, upward flow paths with variable lengths and depths converge near the land surface. This creates a type of mixed flow paths at the same depth. In contrast, in plains, downward flow paths penetrate the thin vadose zone (i.e., with associated shallow water table depths, Figure S6 in Supporting Information S1) and rapidly convert to horizontal flow paths in the saturated zone, showing a type of consistent flow paths at the same depth. Synchronous variations in travel length with ET age in each layer (shown in the second and third rows in Figure 2) or the whole root zone (shown in the first row in Figure 2) indicate that ET water is drawn from similar depths in plains but from contrasting depths in mountainous areas. These differences in the depths of ET water

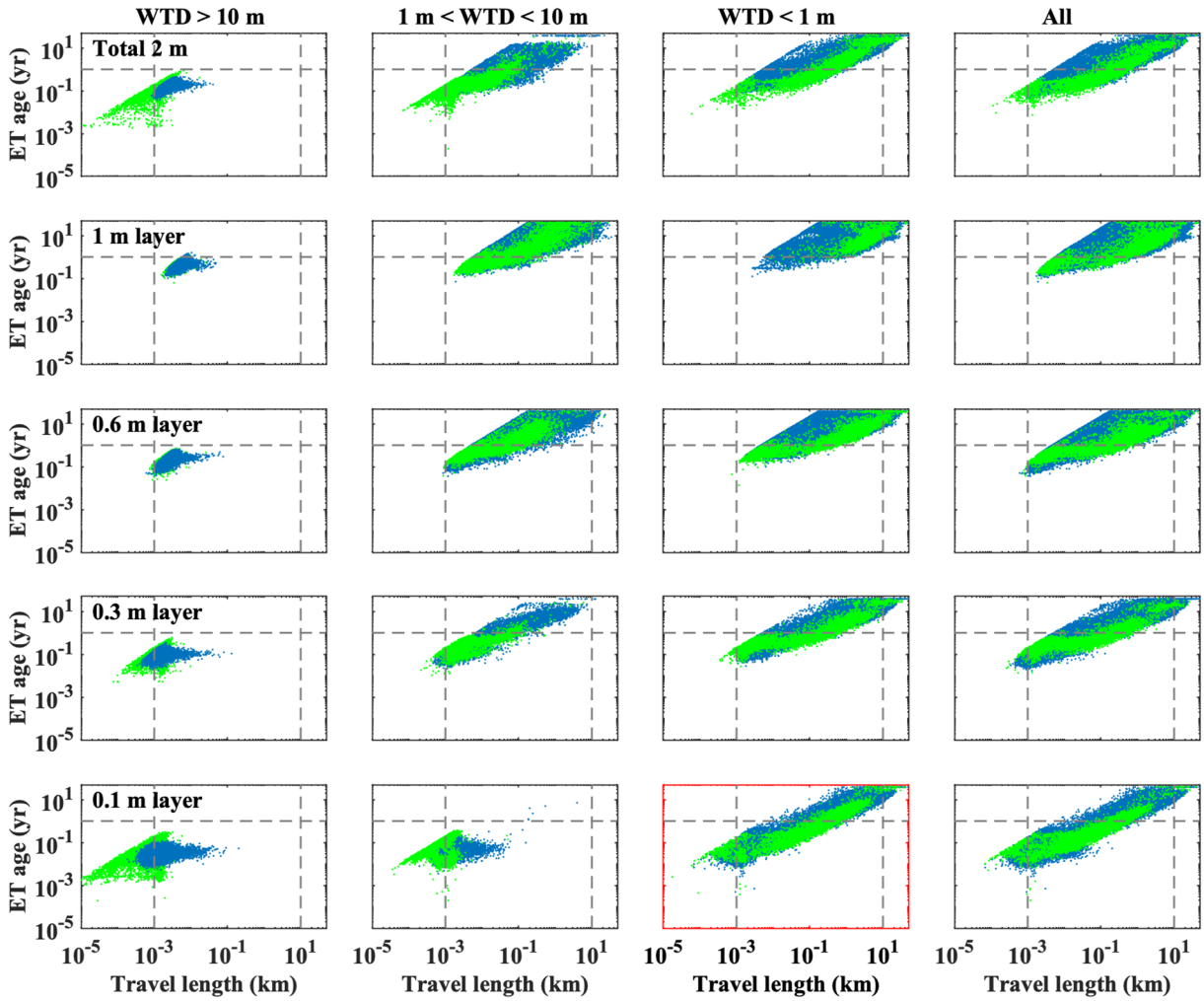

Figure 5. Variations of evapotranspiration (ET) age with subsurface travel length. Blue points are based on spatial distributions of ET age in Figure 1, while green points are based on time series of ET age aggregated in the entire modeling domain (i.e., mountainous areas and plains are not distinguished). The horizontal gray line indicates the ET age of 1 year. The first vertical gray line indicates the travel length of 1 m while the second indicates 10 km. The first row is for the whole root zone, while the second to the fifth are for layers from bottom to top (1.0, 0.6, 0.3, and 0.1 m). The first to the third columns are for subregions with different water table depths (WTDs): WTD > 10 m, 1 m < WTD < 10 m, and WTD < 1 m. The last panel in each row represents the whole layer. The panel for the area with WTD < 1 m in the 0.1 m layer (red rectangle) shows a scaling relationship since ET age varies linearly with travel length in the log-log plot over three orders of magnitude.

sources highlight the topographical controls on ET age. Particularly, the strong fluctuations of ET age associated with fast switches of travel length in the mountainous area, especially in the area with WTD less than 1 m, highlight the heterogeneity of flow paths and the change of the importance of different flow paths with time. The converged deep and long groundwater flow paths dominate the general old ET. Once precipitation happens, the shallow and short flow paths temporarily prevail, leading to young ET. Therefore, ET age in the valley bottom quickly shifts between old and young with precipitation events and has the most significant fluctuations.

Figure 5 shows the relationship between ET age and its subsurface travel length. On mountain ridges (the first column in Figure 5), ET water shows limited movements around a length scale comparable to the thickness of the root zone ($\sim 10^0$ m indicated by the first vertical dash-line). ET age is consequently young, varying in a small range. In the key zone of ET age variations (the second column in Figure 5), the >10 km travel length of ET water (the second vertical dash-line) becomes significant with depth (i.e., from 0.1 to 1 m layer). Travel length of more than 10 km, not possible through pure unsaturated movement in the root zone (Figure S10 in Supporting Information S1), is an indicator of lateral groundwater flow (Text S4 in Supporting Information S1). This suggests that the deeper water source of ET during dry periods is the lateral groundwater flow. Increasing connections with lateral groundwater flow with depth (the second column in Figure 5) shifts ET age in the 0.1 m layer, which is

similar to that on ridges, to about the maximum value (42 years) in this study in the 1 m layer. In valleys (the third column in Figure 5), the travel length of ET water shows a wide range throughout the root zone, highlighting the convergence of variable groundwater flow paths in this subregion, which induces large fluctuations of ET age at subseasonal scales (Figures 2b and 3c). Most notably, a significant scaling relationship (indicated by the red rectangle in Figure 5) between ET age and travel length is shown at the land surface of valleys, where there are the most variable flow paths, as shown in Figure 4.

Our work highlights the importance of accurately describing Tóthian (topography-driven) flow paths in ET age modeling. Three-dimensional variably saturated subsurface flow is essential to capture such topographically induced groundwater flow paths. Traditional land surface models—most without lateral groundwater flow (Clark et al., 2015) and some with simplified lateral groundwater flow (Maneta & Silverman, 2013) may overestimate the drainage in valleys (Fan, 2015) and underestimate the deep flow paths, respectively. Our work supports recent field and modeling evidence of how groundwater in headwaters subsidizes their parent watersheds (Ameli et al., 2018) and related process findings of groundwater subsidy on ET (Hwang et al., 2012).

Some previous work on ET age has shown similar divisions of two subregions (hillslope and valley bottom) based on soil saturation (Soulsby et al., 2016) or soil type (Kuppel et al., 2020). Kuppel et al. (2020) also showed a higher baseline of ET ages with weaker seasonal variability in the valley bottom than on the hillslope, consistent with our results. Fan and others (Fan, 2015; Miguez-Macho & Fan, 2021) delineated two hydrologic subregions: one the upland of precipitation drainage, the other a lowland area of groundwater convergence. They pointed out that plants in the two subregions took different water sources. While we also divided the subregions based on saturation—to show some difference in ET age among subregions—none were as successful as that based on WTDs. This strengthens our point that topography exerts a significant control on ET age variations. Our division based on topography-driven WTDs not only captures the variations in valleys or lowlands but also reveals the necessity to further divide the areas outside the groundwater convergence region.

Additionally, our work extends the critical WTDs ($\sim$1 m < WTD < $\sim$10 m) for energy and water quantity in Kollet and Maxwell (2008) to water age. In this zone, groundwater shows a buffer effect to maintain ET demand and relieves water pressure on plants during dry conditions (Condon et al., 2020). However, our work further showed increased seasonal variability of ET age induced by the old groundwater subsidy. Generally, topography-driven flow paths shape the basic patterns of ET age variations by creating distinct characteristics from ridges to valleys with increasing connections with groundwater, while meteorologic conditions further modulate the basic pattern generating the key zone of ET age variations with WTDs of 1–10 m. However, our large-scale study on basic patterns cannot reject that soil type, geologic unit, land cover, etc. (Figure S2 in Supporting Information S1) affect ET age variations. The topographic controls revealed in our work could be impacted by subvariations of ET age (as seen in Figure 1), possibly regulated by these additional factors. Variations of ET age regulated by additional factors may be locally dominant at finer scales (Allen et al., 2019; Kuppel et al., 2020), but such analysis is beyond the scope of this discussion.

Finally, our GPU-accelerated particle tracking approach that integrates hydrologic modeling with land surface processes enables the explicit analysis of hydrologic compartmentalization (McDonnell, 2017) and its impact on water ages into the water balance. This implementation quantifies how the relatively isolated groundwater can connect with Earth's surface processes at large scales—as we showed here for ET age. Our analysis goes beyond the water quantity work reported in previous studies (de Graaf & Stahl, 2022; Maxwell & Condon, 2016). Our approach is able to reconcile and integrate ET age variations in a unified framework linked to topography-driven flow paths. These topographic controls appear to trump the meteorologic conditions, land cover types, soil types, and geologic units in our modeling domain. Contributions from lateral groundwater flow substantially widen the distributions of ET age showing long tails (Figure S11 in Supporting Information S1). Though ET is a land surface process that is thought to be "shallow and fast," as represented in the current Earth System Models (ESMs) (Fan et al., 2019), our results show the subsurface travel lengths supplying ET water can be over 10 km with corresponding ET ages on the order of tens of years (Figure 5). These will likely increase further with longer simulation times with future developments in high-performance computing. Therefore, our work also illustrates the need to move the simulation of the hydrologic cycle toward the large scale with high-resolution frameworks using advanced parallel architectures (Hokkanen et al., 2021)—especially to accelerate the next-generation ESMs.

Conflict of Interest

The authors declare no conflicts of interest relevant to this study.

Data Availability Statement

ParFlow-CLM (ParFlow Developers, 2022) is open source at https://github.com/parflow, https://doi.org/10.5281/zenodo.6413322; EcoSLIM (Yang et al., 2023a, 2023b) is also open source at https://github.com/aureliayang/EcoSLIM_CONUS, https://doi.org/10.5281/zenodo.7302297.

The inputs scripts for simulations and the Figure data (including Figure data in Supporting Information S1) (Yang, Maxwell, McDonnell, et al., 2022; Yang, Maxwell, & Valent, 2022) can be found at https://doi.org/10.6084/m9.figshare.19566085.

Acknowledgments

This work was supported by the National Natural Science Foundation of China (41807198), by the National Science Foundation under Award 2117393, and by the U.S. Department of Energy, Office of Science, Offices of Advanced Scientific Computing Research and Biological and Environmental Sciences IDEAS project and Watershed Function Scientific Focus Area under Award DE-AC02-05CH11231. The authors acknowledge high-performance computing support from Cheyenne (https://doi.org/10.5065/D6RX99HX) provided by NCAR's Computational and Information Systems Laboratory, sponsored by the National Science Foundation.

References

Allen, S. T., Kirchner, J. W., Braun, S., Siegwolf, R. T. W., & Goldsmith, G. R. (2019). Seasonal origins of soil water used by trees. *Hydrology and Earth System Sciences*, *23*(2), 1199–1210. https://doi.org/10.5194/hess-23-1199-2019

Ameli, A. A., Gabrielli, C., Morgenstern, U., & McDonnell, J. J. (2018). Groundwater subsidy from headwaters to their parent water watershed: A combined field-modeling approach. *Water Resources Research*, *54*, 5110–5125. https://doi.org/10.1029/2017WR022356

Asadollahi, M., Nehemy, M. F., McDonnell, J. J., Rinaldo, A., & Benettin, P. (2022). Toward a closure of catchment mass balance: Insight on the missing link from a vegetated lysimeter. *Water Resources Research*, *58*, e2021WR030698. https://doi.org/10.1029/2021WR030698

Bao, Z. X., Zhang, J. Y., Wang, G. Q., Fu, G. B., He, R. M., Yan, X. L., et al. (2012). Attribution for decreasing streamflow of the Haihe River basin, northern China: Climate variability or human activities? *Journal of Hydrology*, *460*, 117–129. https://doi.org/10.1016/j.jhydrol.2012.06.054

Benettin, P., Nehemy, M. F., Asadollahi, M., Pratt, D., Bensimon, M., McDonnell, J. J., & Rinaldo, A. (2021). Tracing and closing the water balance in a vegetated Lysimeter. *Water Resources Research*, *57*, e2020WR029049. https://doi.org/10.1029/2020WR029049

Botter, G. (2012). Catchment mixing processes and travel time distributions. *Water Resources Research*, *48*, W05545. https://doi.org/10.1029/2011WR011160

Calabrese, S., & Porporato, A. (2017). Multiple outflows, spatial components, and nonlinearities in age theory. *Water Resources Research*, *53*, 110–126. https://doi.org/10.1002/2016WR019227

Cao, G. L., Zheng, C. M., Scanlon, B. R., Liu, J., & Li, W. P. (2013). Use of flow modeling to assess sustainability of groundwater resources in the North China Plain. *Water Resources Research*, *49*, 159–175. https://doi.org/10.1029/2012WR011899

Cardenas, M. B. (2008). Surface water-groundwater interface geomorphology leads to scaling of residence times. *Geophysical Research Letters*, *35*, L08402. https://doi.org/10.1029/2008GL033753

Chu, J. T., Xia, J., Xu, C. Y., & Singh, V. P. (2010). Statistical downscaling of daily mean temperature, pan evaporation and precipitation for climate change scenarios in Haihe River, China. *Theoretical and Applied Climatology*, *99*(1–2), 149–161. https://doi.org/10.1007/s00704-009-0129-6

Clark, M. P., Fan, Y., Lawrence, D. M., Adam, J. C., Bolster, D., Gochis, D. J., et al. (2015). Improving the representation of hydrologic processes in earth system models. *Water Resources Research*, *51*, 5929–5956. https://doi.org/10.1002/2015WR017096

Condon, L. E., Atchley, A. L., & Maxwell, R. M. (2020). Evapotranspiration depletes groundwater under warming over the contiguous United States. *Nature Communications*, *11*(1), 873. https://doi.org/10.1038/s41467-020-14688-0

de Graaf, I. E. M., & Stahl, K. (2022). A model comparison assessing the importance of lateral groundwater flows at global-scale. *Environmental Research Letters*, *17*, 044020. 10.1088/1748-9326/ac50d2

Engdahl, N. B., & Maxwell, R. M. (2014). Approximating groundwater age distributions using simple streamtube models and multiple tracers. *Advances in Water Resources*, *66*, 19–31. https://doi.org/10.1016/j.advwatres.2014.02.001

Fan, Y. (2015). Groundwater in the Earth's critical zone: Relevance to large-scale patterns and processes. *Water Resources Research*, *51*, 3052–3069. https://doi.org/10.1002/2015WR017037

Fan, Y. (2016). How much and how old? *Nature Geoscience*, *9*(2), 93–94. https://doi.org/10.1038/ngeo2609

Fan, Y., Clark, M., Lawrence, D. M., Swenson, S., Band, L. E., Brantley, S. L., et al. (2019). Hillslope hydrology in global change research and earth system modeling. *Water Resources Research*, *55*, 1737–1772. https://doi.org/10.1029/2018WR023903

Fan, Y., Miguez-Macho, G., Jobbágy, E. G., Jackson, R. B., & Otero-Casal, C. (2017). Hydrologic regulation of plant rooting depth. *Proceedings of the National Academy of Sciences of the United States of America*, *114*(40), 10572–10577. https://doi.org/10.1073/pnas.1712381114

Freeze, R. A., & Witherspoon, P. A. (1967). Theoretical analysis of regional groundwater flow: 2. Effect of water-table configuration and subsurface permeability variation. *Water Resources Research*, *3*(2), 623–634. https://doi.org/10.1029/WR003i002p00623

Gleeson, T., Smith, L., Moosdorf, N., Hartmann, J., Durr, H. H., Manning, A. H., et al. (2011). Mapping permeability over the surface of the Earth. *Geophysical Research Letters*, *38*, L02401. https://doi.org/10.1029/2010GL045565

Gleeson, T., Wagener, T., Döll, P., Zipper, S. C., West, C., Wada, Y., et al. (2021). GMD perspective: The quest to improve the evaluation of groundwater representation in continental-to global-scale models. *Geoscientific Model Development*, *14*(12), 7545–7571. https://doi.org/10.5194/gmd-14-7545-2021

Gomez, J. D., & Wilson, J. L. (2013). Age distributions and dynamically changing hydrologic systems: Exploring topography-driven flow. *Water Resources Research*, *49*, 1503–1522. https://doi.org/10.1002/wrcr.20127

Harada, Y., Kamahori, H., Kobayashi, C., Endo, H., Kobayashi, S., Ota, Y., et al. (2016). The JRA-55 reanalysis: Representation of atmospheric circulation and climate variability. *Journal of the Meteorological Society of Japan*, *94*(3), 269–302. https://doi.org/10.2151/jmsj.2016-015

Hersbach, H., Bell, B., Berrisford, P., Biavati, G., Horányi, A., Muñoz Sabater, J., et al. (2018). *ERA5 hourly data on single levels from 1979 to present*. Copernicus Climate Change Service (C3S) Climate Data Store (CDS). https://doi.org/10.24381/cds.adbb2d47

Hokkanen, J., Kollet, S., Kraus, J., Herten, A., Hrywniak, M., & Pleiter, D. (2021). Leveraging HPC accelerator architectures with modern techniques—Hydrologic modeling on GPUs with ParFlow. *Computational Geosciences*, *25*(5), 1579–1590. https://doi.org/10.1007/s10596-021-10051-4

Hwang, T., Band, L. E., Vose, J. M., & Tague, C. (2012). Ecosystem processes at the watershed scale: Hydrologic vegetation gradient as an indicator for lateral hydrologic connectivity of headwater catchments. *Water Resources Research*, *48*, W06514. https://doi.org/10.1029/2011WR011301

Jiang, X.-W., Wan, L., Cardenas, M. B., Ge, S., & Wang, X.-S. (2010). Simultaneous rejuvenation and aging of groundwater in basins due to depth-decaying hydraulic conductivity and porosity. *Geophysical Research Letters*, *37*, L05403. https://doi.org/10.1029/2010GL042387

Kirchner, J. W. (2016a). Aggregation in environmental systems—Part 1: Seasonal tracer cycles quantify young water fractions, but not mean transit times, in spatially heterogeneous catchments. *Hydrology and Earth System Sciences*, *20*(1), 279–297. https://doi.org/10.5194/hess-20-279-2016

Kirchner, J. W. (2016b). Aggregation in environmental systems – Part 2: Catchment mean transit times and young water fractions under hydrologic nonstationarity. *Hydrology and Earth System Sciences*, *20*(1), 299–328. https://doi.org/10.5194/hess-20-299-2016
Knighton, J., Kuppel, S., Smith, A., Soulsby, C., Sprenger, M., & Tetzlaff, D. (2020). Using isotopes to incorporate tree water storage and mixing dynamics into a distributed ecohydrologic modelling framework. *Ecohydrology*, *13*(3), e2201. https://doi.org/10.1002/eco.2201
Kobayashi, S., Ota, Y., Harada, Y., Ebita, A., Moriya, M., Onoda, H., et al. (2015). The JRA-55 reanalysis: General specifications and basic characteristics. *Journal of the Meteorological Society of Japan*, *93*(1), 5–48. https://doi.org/10.2151/jmsj.2015-001
Kollet, S. J., & Maxwell, R. M. (2008). Capturing the influence of groundwater dynamics on land surface processes using an integrated, distributed watershed model. *Water Resources Research*, *44*, W02402. https://doi.org/10.1029/2007WR006004
Kuffour, B. N. O., Engdahl, N. B., Woodward, C. S., Condon, L. E., Kollet, S., & Maxwell, R. M. (2020). Simulating coupled surface–subsurface flows with ParFlow v3.5.0: Capabilities, applications, and ongoing development of an open-source, massively parallel, integrated hydrologic model. *Geoscientific Model Development*, *13*(3), 1373–1397. https://doi.org/10.5194/gmd-13-1373-2020
Kuppel, S., Tetzlaff, D., Maneta, M. P., & Soulsby, C. (2018). EcH(2)O-iso 1.0: Water isotopes and age tracking in a process-based, distributed ecohydrological mode. *Geoscientific Model Development*, *11*(7), 3045–3069. https://doi.org/10.5194/gmd-11-3045-2018
Kuppel, S., Tetzlaff, D., Maneta, M. P., & Soulsby, C. (2020). Critical zone storage controls on the water ages of ecohydrological outputs. *Geophysical Research Letters*, *47*, e2020GL088897. https://doi.org/10.1029/2020GL088897
Maneta, M. P., & Silverman, N. L. (2013). A spatially distributed model to simulate water, energy, and vegetation dynamics using information from regional climate models. *Earth Interactions*, *17*(11), 1–44. https://doi.org/10.1175/2012EI000472.1
Maxwell, R. M., & Condon, L. E. (2016). Connections between groundwater flow and transpiration partitioning. *Science*, *353*(6297), 377–380. https://doi.org/10.1126/science.aaf7891
Maxwell, R. M., Condon, L. E., Danesh-Yazdi, M., & Bearup, L. A. (2019). Exploring source water mixing and transient residence time distributions of outflow and evapotranspiration with an integrated hydrologic model and Lagrangian particle tracking approach. *Ecohydrology*, *12*(1), e2042. https://doi.org/10.1002/eco.2042
Maxwell, R. M., Condon, L. E., & Kollet, S. J. (2015). A high-resolution simulation of groundwater and surface water over most of the continental US with the integrated hydrologic model ParFlow v3. *Geoscientific Model Development*, *8*(3), 923–937. https://doi.org/10.5194/gmd-8-923-2015
Maxwell, R. M., Condon, L. E., Kollet, S. J., Maher, K., Haggerty, R., & Forrester, M. M. (2016). The imprint of climate and geology on the residence times of groundwater. *Geophysical Research Letters*, *43*, 701–708. https://doi.org/10.1002/2015GL066916
Maxwell, R. M., & Miller, N. L. (2005). Development of a coupled land surface and groundwater model. *Journal of Hydrometeorology*, *6*(3), 233–247. https://doi.org/10.1175/jhm422.1
McDonnell, J. J. (2017). Beyond the water balance. *Nature Geoscience*, *10*(6), 396. https://doi.org/10.1038/ngeo2964
Miguez-Macho, G., & Fan, Y. (2021). Spatiotemporal origin of soil water taken up by vegetation. *Nature*, *598*(7882), 624–628. https://doi.org/10.1038/s41586-021-03958-6
Nehemy, M. F., Benettin, P., Asadollahi, M., Pratt, D., Rinaldo, A., & McDonnell, J. J. (2021). Tree water deficit and dynamic source water partitioning. *Hydrological Processes*, *35*(1), e14004. https://doi.org/10.1002/hyp.14004
ParFlow Developers. (2022). parflow/parflow: ParFlow Version 3.11.0 (v3.11.0) [Software]. Zenodo. https://doi.org/10.5281/zenodo.7055486
Rabus, B., Eineder, M., Roth, A., & Bamler, R. (2003). The shuttle radar topography mission - A new class of digital elevation models acquired by spaceborne radar. *ISPRS Journal of Photogrammetry and Remote Sensing*, *57*(4), 241–262. https://doi.org/10.1016/S0924-2716(02)00124-7
Rahimpour Asenjan, M., & Danesh-Yazdi, M. (2020). The effect of seasonal variation in precipitation and evapotranspiration on the transient travel time distributions. *Advances in Water Resources*, *142*, 103618. https://doi.org/10.1016/j.advwatres.2020.103618
Rodriguez, N. B., Benettin, P., & Klaus, J. (2020). Multimodal water age distributions and the challenge of complex hydrological landscapes. *Hydrological Processes*, *34*(12), 2707–2724. https://doi.org/10.1002/hyp.13770
Schlesinger, W. H., & Jasechko, S. (2014). Transpiration in the global water cycle. *Agricultural and Forest Meteorology*, *189*, 115–117. https://doi.org/10.1016/j.agrformet.2014.01.011
Shangguan, W., Dai, Y., Liu, B., Ye, A., & Yuan, H. (2012). A soil particle-size distribution dataset for regional land and climate modelling in China. *Geoderma*, *171–172*, 85–91. https://doi.org/10.1016/j.geoderma.2011.01.013
Soulsby, C., Birkel, C., & Tetzlaff, D. (2016). Characterizing the age distribution of catchment evaporative losses. *Hydrological Processes*, *30*(8), 1308–1312. https://doi.org/10.1002/hyp.10751
Sprenger, M., Stumpp, C., Weiler, M., Aeschbach, W., Allen, S. T., Benettin, P., et al. (2019). The demographics of water: A review of water ages in the critical zone. *Reviews of Geophysics*, *57*, 800–834. https://doi.org/10.1029/2018RG000633
Sprenger, M., Tetzlaff, D., Buttle, J., Laudon, H., & Soulsby, C. (2018). Water ages in the critical zone of long-term experimental sites in northern latitudes. *Hydrology and Earth System Sciences*, *22*(7), 3965–3981. https://doi.org/10.5194/hess-22-3965-2018
Tóth, J. (1963). A theoretical analysis of groundwater flow in small drainage basins. *Journal of Geophysical Research*, *68*(16), 4795–4812. https://doi.org/10.1029/JZ068i016p04795
USGS. (2018). *Global land cover characterization*. United States Geological Survey. https://doi.org/10.5066/F7GB230D
Wang, S. Q., Yuan, R. Q., Tang, C. Y., Song, X. F., Currell, M., Yang, Z. L., & Sheng, Z. P. (2018). Combination of CFCs and stable isotopes to characterize the mechanism of groundwater-surface water interactions in a headwater basin of the North China Plain. *Hydrological Processes*, *32*(11), 1571–1587. https://doi.org/10.1002/hyp.11494
Wilusz, D. C., Harman, C. J., Ball, W. B., Maxwell, R. M., & Buda, A. R. (2019). Using particle tracking to understand flow paths, age distributions, and the paradoxical origins of the inverse storage effect in an experimental catchment. *Water Resources Research*, *56*, e2019WR025140. https://doi.org/10.1029/2019WR025140
Yang, C., Li, H.-Y., Fang, Y., Cui, C., Wang, T., Zheng, C., et al. (2020). Effects of groundwater pumping on ground surface temperature: A regional modeling study in the North China plain. *Journal of Geophysical Research: Atmospheres*, *125*, e2019JD031764. https://doi.org/10.1029/2019JD031764
Yang, C., Maxwell, R., McDonnell, J., Yang, X., & Tijerina-Kreuzer, D. (2022). The role of topography in controlling evapotranspiration age (Version 1.0) [Dataset]. figshare. https://doi.org/10.6084/m9.figshare.19566085.v1
Yang, C., Maxwell, R. M., & Valent, R. (2022). Accelerating the Lagrangian simulation of water ages on distributed, multi-GPU platforms: The importance of dynamic load balancing. *Computers & Geosciences*, *166*, 105189. https://doi.org/10.1016/j.cageo.2022.105189
Yang, C., Ponder, C., Wang, B., Tran, H., Zhang, J., Swilley, J., et al. (2023a). Accelerating the Lagrangian particle tracking in hydrologic modeling to continental-scale. *Journal of Advances in Modeling Earth Systems*, *15*, e2022MS003507. https://doi.org/10.1029/2022MS003507
Yang, C., Ponder, C., Wang, B., Tran, H., Zhang, J., Swilley, J., et al. (2023b). EcoSLIM_CONUS: November 8, 2022 release (Version 1.0) [Software]. Zenodo. https://doi.org/10.5281/zenodo.7302297

Yang, C., Zhang, Y.-K., Liang, X., Olschanowsky, C., Yang, X., & Maxwell, R. (2021). Accelerating the Lagrangian particle tracking of residence time distributions and source water mixing towards large scales. *Computers & Geosciences*, *151*, 104760. https://doi.org/10.1016/j.cageo.2021.104760

Zhang, J., Wang, X.-S., Yin, L., Wang, W., Love, A., Lu, Z.-T., et al. (2021). Inflection points on groundwater age and geochemical profiles along wellbores light up hierarchically nested flow systems. *Geophysical Research Letters*, *48*, e2020GL092337. https://doi.org/10.1029/2020GL092337

Zheng, H. X., Liu, X. M., Liu, C. M., Dai, X. Q., & Zhu, R. R. (2009). Assessing contributions to panevaporation trends in Haihe River Basin, China. *Journal of Geophysical Research*, *114*, D24105. https://doi.org/10.1029/2009JD012203

References From the Supporting Information

Asante, K. O., Artan, G. A., Pervez, M. S., Bandaragoda, C., & Verdin, J. P. (2008). *Technical manual for the geospatial stream flow model (GeoSFM). (Open-File Rep. 2007-1441)*. United States Geological Survey. Retrieved from http://pubs.er.usgs.gov/publication/ofr20071441

Beven, K., & Germann, P. (2013). Macropores and water flow in soils revisited. *Water Resources Research*, *49*, 3071–3092. https://doi.org/10.1002/wrcr.20156

Condon, L. E., Kollet, S., Bierkens, M. F. P., Fogg, G. E., Maxwell, R. M., Hill, M. C., et al. (2021). Global groundwater modeling and monitoring: Opportunities and challenges. *Water Resources Research*, *57*, e2020WR029500. https://doi.org/10.1029/2020WR029500

Condon, L. E., Markovich, K. H., Kelleher, C. A., McDonnell, J. J., Ferguson, G., & McIntosh, J. C. (2020). Where is the bottom of a watershed? *Water Resources Research*, *56*, e2019WR026010. https://doi.org/10.1029/2019WR026010

Condon, L. E., & Maxwell, R. M. (2014). Feedbacks between managed irrigation and water availability: Diagnosing temporal and spatial patterns using an integrated hydrologic model. *Water Resources Research*, *50*, 2600–2616. https://doi.org/10.1002/2013WR014868

Condon, L. E., & Maxwell, R. M. (2017). Systematic shifts in Budyko relationships caused by groundwater storage changes. *Hydrology and Earth System Sciences*, *21*(2), 1117–1135. https://doi.org/10.5194/hess-21-1117-2017

Condon, L. E., & Maxwell, R. M. (2019a). Modified priority flood and global slope enforcement algorithm for topographic processing in physically based hydrologic modeling applications. *Computers & Geosciences*, *126*, 73–83. https://doi.org/10.1016/j.cageo.2019.01.020

Condon, L. E., & Maxwell, R. M. (2019b). Simulating the sensitivity of evapotranspiration and streamflow to large-scale groundwater depletion. *Science Advances*, *5*(6), eaav4574. https://doi.org/10.1126/sciadv.aav4574

Dai, Y. J., Zeng, X. B., Dickinson, R. E., Baker, I., Bonan, G. B., Bosilovich, M. G., et al. (2003). The common land model. *Bulletin of the American Meteorological Society*, *84*(8), 1013–1023. https://doi.org/10.1175/Bams-84-8-1013

Engdahl, N. B., & Maxwell, R. M. (2015). Quantifying changes in age distributions and the hydrologic balance of a high-mountain watershed from climate induced variations in recharge. *Journal of Hydrology*, *522*, 152–162. https://doi.org/10.1016/j.jhydrol.2014.12.032

Fan, Y., Miguez-Macho, G., Weaver, C. P., Walko, R., & Robock, A. (2007). Incorporating water table dynamics in climate modeling: 1. Water table observations and equilibrium water table simulations. *Journal of Geophysical Research*, *112*, D10125. https://doi.org/10.1029/2006JD008111

Ferguson, I. M., Jefferson, J. L., Maxwell, R. M., & Kollet, S. J. (2016). Effects of root water uptake formulation on simulated water and energy budgets at local and basin scales. *Environmental Earth Sciences*, *75*(4), 316. https://doi.org/10.1007/s12665-015-5041-z

Ferguson, I. M., & Maxwell, R. M. (2011). Hydrologic and land-energy feedbacks of agricultural water management practices. *Environmental Research Letters*, *6*(1), 014006. https://doi.org/10.1088/1748-9326/6/1/014006

Foster, L., & Maxwell, R. (2019). Sensitivity analysis of hydraulic conductivity and Manning's n parameters lead to new method to scale effective hydraulic conductivity across model resolutions. *Hydrological Processes*, *33*(3), 332–349. https://doi.org/10.1002/hyp.13327

Glaser, B., Jackisch, C., Hopp, L., & Klaus, J. (2019). How meaningful are plot-scale observations and simulations of preferential flow for catchment models? *Vadose Zone Journal*, *18*(1), 1–18. https://doi.org/10.2136/vzj2018.08.0146

Hartick, C., Furusho-Percot, C., Goergen, K., & Kollet, S. (2021). An interannual probabilistic assessment of subsurface water storage over Europe using a fully coupled terrestrial model. *Water Resources Research*, *57*, e2020WR027828. https://doi.org/10.1029/2020WR027828

Hendrickx, J., & Flury, M. (2001). *Uniform and preferential flow mechanisms in the vadose zone* (pp. 149–187). National Research Council, National Academy Press.

Hopp, L., Glaser, B., Klaus, J., & Schramm, T. (2020). The relevance of preferential flow in catchment scale simulations: Calibrating a 3D dual-permeability model using DREAM. *Hydrological Processes*, *34*(5), 1237–1254. https://doi.org/10.1002/hyp.13672

Hu, M. P., Zhang, Y. F., Wu, K. B., Shen, H., Yao, M. Y., Dahlgren, R. A., & Chen, D. J. (2020). Assessment of streamflow components and hydrologic transit times using stable isotopes of oxygen and hydrogen in waters of a subtropical watershed in eastern China. *Journal of Hydrology*, *589*, 125363. https://doi.org/10.1016/j.jhydrol.2020.125363

Jefferson, J. L., & Maxwell, R. M. (2015). Evaluation of simple to complex parameterizations of bare ground evaporation. *Journal of Advances in Modeling Earth Systems*, *7*, 1075–1092. https://doi.org/10.1002/2014MS000398

Jefferson, J. L., Maxwell, R. M., & Constantine, P. G. (2017). Exploring the sensitivity of photosynthesis and stomatal resistance parameters in a land surface model. *Journal of Hydrometeorology*, *18*(3), 897–915. https://doi.org/10.1175/JHM-D-16-0053.1

Keune, J., Gasper, F., Goergen, K., Hense, A., Shrestha, P., Sulis, M., & Kollet, S. (2016). Studying the influence of groundwater representations on land surface-atmosphere feedbacks during the European heat wave in 2003. *Journal of Geophysical Research: Atmospheres*, *121*, 13301–13325. https://doi.org/10.1002/2016JD025426

Kollet, S. J., & Maxwell, R. M. (2006). Integrated surface-groundwater flow modeling: A free-surface overland flow boundary condition in a parallel groundwater flow model. *Advances in Water Resources*, *29*(7), 945–958. https://doi.org/10.1016/j.advwatres.2005.08.006

Lin, P., Pan, M., Beck, H. E., Yang, Y., Yamazaki, D., Frasson, R., et al. (2019). Global reconstruction of naturalized river flows at 2.94 million reaches. *Water Resources Research*, *55*, 6499–6516. https://doi.org/10.1029/2019WR025287

Maurer, E. P., Wood, A. W., Adam, J. C., Lettenmaier, D. P., & Nijssen, B. (2002). A long-term hydrologically based dataset of land surface fluxes and states for the conterminous United States. *Journal of Climate*, *15*(22), 3237–3251. https://doi.org/10.1175/1520-0442(2002)015<3237:ALTHBD>2.0.CO;2

Maxwell, R. M. (2013). A terrain-following grid transform and preconditioner for parallel, large-scale, integrated hydrologic modeling. *Advances in Water Resources*, *53*, 109–117. https://doi.org/10.1016/j.advwatres.2012.10.001

Ryken, A., Bearup, L. A., Jefferson, J. L., Constantine, P., & Maxwell, R. M. (2020). Sensitivity and model reduction of simulated snow processes: Contrasting observational and parameter uncertainty to improve prediction. *Advances in Water Resources*, *135*, 103473. https://doi.org/10.1016/j.advwatres.2019.103473

Stewart, M. K., Morgenstern, U., & McDonnell, J. J. (2010). Truncation of stream residence time: How the use of stable isotopes has skewed our concept of streamwater age and origin. *Hydrological Processes*, *24*(12), 1646–1659. https://doi.org/10.1002/hyp.7576

Toth, J. (1963). A theoretical analysis of groundwater flow in small drainage basins. *Journal of Geophysical Research*, *68*(16), 4795–4812. https://doi.org/10.1029/JZ068i016p04795

Tran, H., Zhang, J., Cohard, J.-M., Condon, L. E., & Maxwell, R. M. (2020). Simulating groundwater-streamflow connections in the upper Colorado River Basin. *Groundwater*, *58*(3), 392–405. https://doi.org/10.1111/gwat.13000

Tran, H., Zhang, J., O'Neill, M. M., Ryken, A., Condon, L. E., & Maxwell, R. M. (2022). A hydrological simulation dataset of the Upper Colorado River Basin from 1983 to 2019. *Scientific Data*, *9*(1), 16. https://doi.org/10.1038/s41597-022-01123-w

Yamazaki, D., Ikeshima, D., Sosa, J., Bates, P. D., Allen, G. H., & Pavelsky, T. M. (2019). MERIT hydro: A high-resolution global hydrography map based on latest topography dataset. *Water Resources Research*, *55*, 5053–5073. https://doi.org/10.1029/2019WR024873

Zhang, J., Condon, L. E., Tran, H., & Maxwell, R. M. (2021). A national topographic dataset for hydrological modeling over the contiguous United States. *Earth System Science Data*, *13*(7), 3263–3279. https://doi.org/10.5194/essd-13-3263-2021